Shahid Chamran University of Ahvaz

Iranian Association of Electrical and Electronics Engineers

Journal of Applied Research in Electrical Engineering

E-ISSN: 2783-2864
P-ISSN: 2717-414X
Homepage: https://jaree.scu.ac.ir/

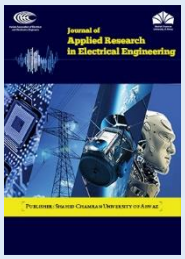

Research Article

Sizing Equations of Axial Flux Permanent Magnet (AFPM) Machine Based on an Analytical Method

Hamid Radmanesh*

Electrical Engineering Department, Shahid Sattari Aeronautical University of Science and Technology, Tehran 15916-34311, Iran

** Corresponding Author: radmanesh@ssau.ac.ir*

Abstract: This paper presents a new algorithm for sizing equations of an Axial Flux Permanent Magnet (AFPM) machine based on an analytical method. To obtain a better performance, the dimensions of the stator and rotor cores are calculated. It is shown that the magnetic flux densities throughout these cores remain closed to the flux density of the B-H curve knee point of the ferromagnetic material characteristics. A new algorithm is proposed to determine the dimensions of the different parts of the machine, and it is used to calculate the height of the permanent magnet precisely. To show the effectiveness of the suggested algorithm, a sample AFPM machine is designed based on sizing equations, and Finite Element Analysis (FEA) is employed to validate these design formulas. A complete simulation study is accomplished, and some of the results are presented to confirm the accuracy of the sizing equations.

Keywords: Axial Flux Permanent Magnet (AFPM), sizing equations, design algorithm, Finite Element Analysis (FEA).

Article history
Received 02 July 2019; Revised 22 June 2020; Accepted 1 July 2020; Published online 10 July 2020.

How to cite this article
Hamid Radmanesh, "Sizing equations of axial flux permanent magnet (AFPM) machine based on an analytical method," *J. Appl. Res. Electr. Eng.*, vol. 1, no. 1, pp. 14-21, 2021. DOI: 10.22055/jaree.2020.30169.1000

Check for updates

1. INTRODUCTION

Recently, the applications of Permanent Magnet (PM) motors in industries have been increased due to their excellent performance, sufficient torque, and low noise capability. On the other hand, reducing the prices of PM materials and power electronic devices directly affects the final prices of the PM motors and increases the use of these types of motors in various applications [1]. PM motors are divided into three categories, including Axial Flux (AF), Radial Flux (RF), and Transverse Flux (TF), depending on the direction of the air gap flux motion. The AFPM motor structure is a disc-shaped motor in which the axial motion of the air gap flux causes outstanding features, such as high torque density and excellent efficiency [2]. Besides, AFPM machine structures are varied in terms of the number of rotor and stator discs and stator structures. There are different structures for the stators of this motor, e.g. slotted stator, slotless stator, and coreless stator. These various structures of AFPM motors have quite different performance characteristics. One of the most important performance differences between these types of motors is torque fluctuations. The most important disadvantage of the slotted AFPM motors is their large cogging torques. There are various methods, e.g., skewing PM [3, 4] and manufacturing slotless [3, 5] or coreless structures, that are used to reduce torque fluctuations and noise of the motor. Since PM skewing has no significant impact on the reduction of torque fluctuations, the slotless stator structure is used to significantly reduce torque fluctuations.

Based on the above explanation, AFPM motors have a large variety in terms of the number of rotors and stators, but double-sided structures are widely applicable [6-9]. Based on the position of the rotor and stator, double-sided structures are classified into two categories, i.e., axial-flux interior-rotor (AFIR) and TORUS structures [10-12]. The AFIR structure has two stators and one rotor placed between the two stators' discs. The TORUS structure has two rotors and one stator placed between the two rotor discs. Because of the simplicity of the manufacturing process and the efficient use of coils and stator core, AFPM motors with TORUS structures have widely been used.

In [13], several ways for skewing PM have been presented to minimize axial flux PM motor cogging torque. This paper has investigated the amount of cogging torque reduction related to the amount of permanent magnet skewing and its geometry. According to the results, the use of skewed PM instead of conventional PM reduces the amount of torque cogging dramatically.

Axial flux PM motors with surface-mounted magnets and without stator core have more efficiency and less axial length than motors with a stator core. The motor presented in [14] has an internal magnet, spoke rotor, and variable air gap that cause sinusoidal waveform of the back EMF. The simulation results reveal that by increasing air gap flux density, the presented motor has higher power density and torque density than conventional motors with surface-mounted magnets.

In [15], an improved magnetic equivalent circuit of a synchronous generator has been used to design a coreless axial flux PM generator with two rotors and one stator and with a direct connection for wind turbines. The rotor saturation is also considered in the introduced equivalent circuit. The multi-objective optimization algorithm PSO has been used to optimize the generator. The design objectives are minimizing the cost of materials used in the generator and maximizing the efficiency of annual energy.

In [16], two methods of PM shift and asymmetric magnet have been used to reduce the amount of motor cogging torque. The results show that the simultaneous use of two methods of magnet skewing and magnet shifting has a significant impact on reducing the amount of cogging torque. These two methods are applicable without adding any complexity to the manufacturing process and changing the structure of the motor. Also, the results show that it is possible to design an axial flux PM motor with small cogging torque and almost sinusoidal back EMF with integer coefficients q.

In [17], an axial flux PM motor with a trapezoidal stator core has been introduced and optimally designed. The optimization objective is maximizing efficiency and minimizing motor volume. Also, the motor with a power of 250-1000 W has been designed and compared. The results show that at the same power and efficiency levels, the motor with a trapezoidal core and a winding angle larger than the PM angle has a smaller volume.

In [18], the equivalent circuit of axial flux PM machine has been introduced. In this equivalent circuit, the magnetic saturation, the leakage flux, the armature reaction, and the rotation of the rotor have been considered. The air gap flux density, the back EMF waveform, and the rotor average torque can be calculated by this equivalent circuit. The magnetic equivalent circuit has a small computational size, which facilitates the use of optimized algorithms.

In [19], an analytical method has been presented to determine the sinusoidal magnet shape in an axial flux PM machine with a speed of 1,000,000 RPM for use in the flywheel. The back EMF waveforms have been investigated for both distributed and centralized windings. The results show that the use of a sinusoidal magnet causes sinusoidal back EMF and thus a reduction of the output torque fluctuations. Also, the concentrated winding back EMF has a bigger main component and THD than distributed winding.

This paper uses a particle swarm optimization (PMO)-based method to optimally design a TORUS axial flux motor. In this design, process design variables of the electric motor (the number of pole pairs, input voltage, air gap flux density, air gap length, the ratio of internal to external diameter of the motor, ratio of pole arc to pole pitch, and electrical loading) are employed to reduce the consumed magnet volume and Total Harmonic Distortion (THD) of back Electro Magnetic Field (EMF). The results of the presented sizing equations and PSO algorithm are validated by using FEM simulation results.

PM motors are always proposed as a substitute for conventional induction motors, but their higher prices compared to induction motors are the main reason that makes this type of motor be used to a lesser extent. Since the price difference between these two types of motors is often due to the use of PM, this paper considers the minimization of the PM amount a design optimization objective function.

This paper is organized as follows. Section 2 presents the sizing equations of a slotless AFPM machine. Section 3 discusses the proposed design algorithm. Then, FEM software is applied in Section 4 to investigate the operational behavior of the suggested model, and the related simulation results are analyzed. Finally, comparative cost analysis and conclusion are given.

2. SIZING EQUATIONS OF A SLOTLESS AFPM MACHINE

The flux path in non-slotted AFPM machines is shown in Fig. 1. By studying the flux path, the sizing equations of this machine can be derived.

By neglecting leakage inductance and winding resistance, the output power of the machine is obtained as follows [7, 8]:

$$P_{out} = \eta \frac{m}{T} \int_{.}^{T} e(t) i(t) dt = m K_p \eta E_{pk} I_{pk} \quad (1)$$

where η, m, $e(t)$, $i(t)$, K_p, E_{pk}, and I_{pk} are efficiency, number of phases, the instantaneous value of the induction voltage, the instantaneous value of the phase current, electrical power waveform factor, the maximum value of the back EMF and the maximum value of the phase current, respectively. K_p can be calculated from the following equation:

$$K_p = \frac{1}{T} \int_{.}^{T} \frac{e_{(t)} i_{(t)}}{E_{pk} I_{pk}} dt \quad (2)$$

If a conductor is placed inside a time-varying magnetic field, the voltage will be induced in the conductor. The induced voltage in the conductor is calculated by

$$E_p = V \times l B_{gp} K_w \quad (3)$$

where V is the speed of conductor motion or the rate of the flux density variation, l is the length of the conductor, B_{gp} is the maximum flux density, and K_w is the winding coefficient. By using Eq. (3), the voltage induced in the TORUS axial flux permanent magnet motor can be obtained. In this type of

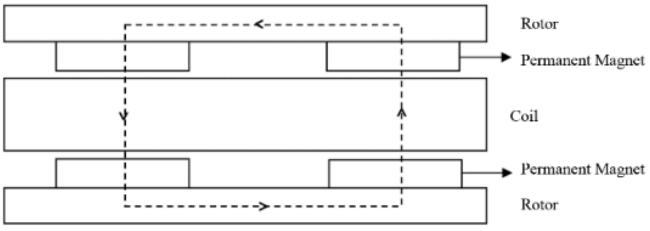

Fig. 1: Flux path in AFPM coreless

machine, the values of l and V can be calculated as follows:

$$V = \frac{D_o(1+\lambda)\pi}{4p} f \tag{4}$$

$$l = 4N_{ph} \frac{D_o(1-\lambda)}{2} \tag{5}$$

By substituting Eq. (4) and (5) in (3), we have:

$$E_p = K_e N_{ph} B_{gp} \frac{f}{p}(1-\lambda^2) D_o^2 \tag{6}$$

where K_e is the EMF coefficient, p is the number of pole pairs, D_o is the outer diameter of the stator, B_{gp} is the maximum flux density in the air gap, and λ is the ratio of inner diameter to the outer diameter of the machine. The rms value of the phase current of the stator winding is obtained by using the following equation:

$$I_{rms} = \frac{A\pi D_{ave}}{2mN_{ph}} \tag{7}$$

where A and D_{ave} are electrical loading and average diameter of the stator, respectively. D_{ave} can be calculated by

$$D_{ave} = D_o \frac{1+\lambda}{2} \tag{8}$$

By substituting Eq. (8) in Eq. (7), the peak value of the current is obtained as follows:

$$I_{pk} = \frac{A\pi}{2mN_{ph}} D_o \frac{1+\lambda}{2} K_i \tag{9}$$

where K_i is the current waveform factor, which is calculated by using the following equation:

$$K_i = \frac{I_{pk}}{I_{rms}} = \frac{1}{\sqrt{\frac{1}{T}\int_0^T (\frac{i_{(t)}}{I_{pk}})^2 dt)}} \tag{10}$$

By substituting Eq. (6) and (9) in (1) and simplifying the final equation, the outer diameter of the stator is obtained as follows:

$$D_o = \sqrt{(\frac{P_{out}}{\frac{\pi}{2}\eta m K_e K_i K_p B_{gp} A \frac{f}{p}(1-\lambda^2)\frac{1+\lambda}{2}\cos(\varphi)})} \tag{11}$$

The saturation phenomenon increases the core losses of the machine. Therefore, the axial length of the stator and rotor cores should be calculated so that the fever local saturation occurs in the cores. On the other hand, to reduce machine weight and cost, the core should be as small as possible. Therefore, the axial length of the core must be determined so that the flux density of the core becomes close to the flux density of the B-H curve knee point of the core ferromagnetic material.

By formulating the flux passing through the air gap and flux inside the core and simplifying it, the axial length of the stator core is obtained as follows:

$$L_{cs} = \frac{B_{gp} K_a \pi D_o (1+\lambda)}{4pB_{cs}} \tag{12}$$

where L_{cs} is the axial length of the stator core, B_{cs} is the maximum flux density in the stator core, and K_a is the ratio of the average flux density to the maximum flux density in the air gap.

In addition, by formulating the flux passing through the rotor core and the magnet flux, the axial length of the rotor core is calculated as follows:

$$L_{cr} = \frac{B_u \pi D_o (1+\lambda)}{8pB_{cr}} \tag{13}$$

where L_{cr} is the axial length of the rotor core and B_u is the ratio of air gap flux density to the leakage factor. The thickness of the stator winding increases the effective air gap length and consequently increases the axial length of the machine. In slotless AFPM machines, the inner diameter of the machine limits the number of wires placed next to each other and in some cases, the wires are wrapped on one another due to space constraint. For this reason, the thickness of the winding layer is dependent on the inner diameter of the machine. The thickness of the winding layer in slotless AFPM machines can be calculated by using the following equation:

$$W_{cu} = \frac{D_o\lambda - \sqrt{(D_o\lambda) - \frac{12}{\pi K_{cu}} N_{ph} A_{cu}}}{2} \tag{14}$$

where A_{cu} is the cross-section of the wire, N_{ph} is the number of turns per phase, and K_{cu} is the coil fill factor.

To produce flux in the air gap, a PM is used because its thickness is dependent on the desired flux density in the air gap, the air gap length, and the thickness of stator winding. Various methods are used to calculate the length of the magnet, but in most research projects, Eq. (15) is used to calculate the thickness of the magnet. In this equation, the important influence of the magnet width on the thickness of the magnet is neglected, which reduces design accuracy [2].

$$L_{pm} = \frac{\mu_r B_g}{B_r - \frac{B_{gp}}{K_d}} K_c (g + W_{cu}) \tag{15}$$

where W_{cu}, g, and L_{pm} are the thickness of the stator winding, the air gap length, and the thickness of the magnets, respectively.

The following equation can be used recursively to exactly calculate the magnet thickness [10,11]:

$$B_{pm} = -\sum_{n=1,3,5,\ldots}^{\infty} \frac{B_1}{B_2} \cos(\frac{n\pi x}{t_p}) \tag{16}$$

where

$$B_1 = \frac{8B_r}{n\pi}\sin(\frac{\alpha n\pi}{2})e^{-\frac{n\pi(g+w_{cu})}{t_p}} \quad (17)$$

$$B_2 = (e^{-\frac{2n\pi(g+w_{cu})}{t_p}}+1) + \frac{\mu_r(-e^{-\frac{2n\pi(g+w_{cu})}{t_p}}+1)}{e^{\frac{2n\pi L_{pm}}{t_p}}-1} \times(e^{\frac{2n\pi L_{pm}}{t_p}}+1) \quad (18)$$

where t_p, B_r, and α are pole pitch, the residual flux density of the magnet, and the ratio of the pole arc to the pole pitch, respectively. Also, the power density of the machine, i.e., the ratio of the output power to the machine volume can be calculated using the following equation:

$$P_{den} = \frac{P_{out}}{\frac{\pi}{4}D_o^2 L_{tot}} \quad (19)$$

where L_{tot} is the axial length of the machine obtained by

$$L_{tot} = L_{cs} + 2L_{cr} + 2W_{cu} + 2g + 2L_{pm} \quad (20)$$

By using the extracted sizing equations and the PSO algorithm, the desired electric motor can be designed.

3. Proposed Design Algorithm

By using the above equations, a design algorithm is proposed for slotless AFPM machines. The flowchart of the proposed algorithm is shown in Fig. 2. According to this flowchart, the overall machine design limitations, such as axial length, outer diameter, and efficiency of the machine, are first determined. In the machine design, some design parameters are optionally determined and the values of the other parameters (unknown problems) are calculated from these optional parameters. In the second step, the values of these optional parameters are determined independently of the other parameters.

Then, the dimensions and computational parameters are obtained based on the equations presented in Section 2. The most important point in the proposed design flowchart is the calculation of the air gap flux density by using Eq. (16).

The flux density, which is obtained from this equation, is compared with the reference value. In the case of inequality of these two values, the thickness of the PM is increased or decreased until these two values become equal. In this case, the exact thickness of the magnet is obtained to generate the desired flux density in the air gap. The objective function of the optimization algorithm is then calculated. This design process is repeated until the objective function is met, and the design algorithm converges. The results of the design algorithm are presented in the following sections.

4. Simulation Results

To validate the equations presented in the previous section, these equations are used to design a sample slotless AFPM machine. The list of the materials used in different parts of the machine is listed in Table 1. Due to the lack of slots in the stator core, it is possible to distribute the arm of each coil in the stator periphery. This has a direct effect on the THD amount of the induced voltage in the windings. To illustrate this issue, motors with different stator winding distribution are designed. By using the equations presented in this paper, the dimensions of these machines are determined. Table 2 presents the basic dimensions and the parameters of the designed machines. According to the parameters in this table, the designed motor with 60° electrical distributed coil has better performance characteristics compared to the other three motors.

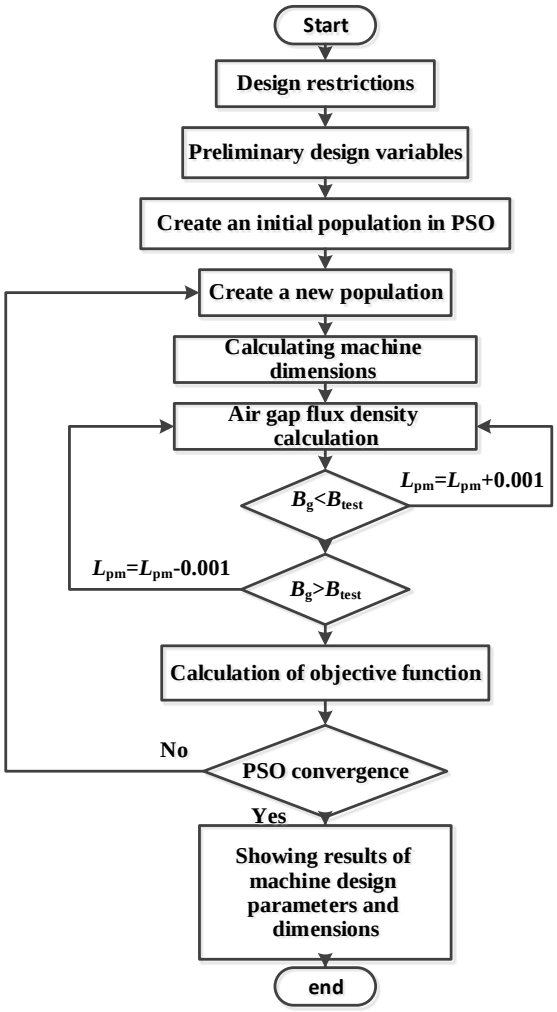

Fig. 2: The flowchart of the machine design process

Table 1: The materials used in different parts of the machine

Permanent magnet	N45
Stator core type	50A470
Rotor core type	50JN400
Coil type	Copper

Table 2: The basic dimensions and parameters of the designed machines with different stator winding distributions

Coil distribution (Electrical degrees)	PM_{den} (cm^3)	D_o (mm)	V_L (V)	THD Back EMF	A
60	21.048	161.692	107.314	6.4031	25571
54	23.345	155.371	161.784	6.5018	28897
42	27.145	175.843	115.271	8.5723	19963
30	35.846	179.091	146.289	9.8065	19047
L_{pm} (mm)	L_{cs} (mm)	L_{cr} (mm)	B_g (T)	α	λ
2.872	10.078	5.8875	0.35	0.699	0.7
3.463	12.101	7.0662	0.35	0.697	0.7
3.137	10.957	6.3974	0.35	0.698	0.7
3.988	13.913	8.1064	0.349	0.699	0.7

Further analyses are done on this type of motor. The optimization objective function of the electrical machine is one of the most important parts of the design process. So, by changing the optimization objective function, the dimensions and performance characteristics of the machine can be changed significantly. The optimization objective function is determined based on the application type of the machine, consumer demands, and mechanical and magnetic constraints. Considering the AFPM motors with better performance characteristics in comparison with the conventional induction motors, it is possible to introduce this type of PM machines as a substitute alternative for conventional induction motors.

But, due to the use of PM in AFPM motors and the high price of this type of material, AFPM motors are more expensive compared to conventional induction motors. Therefore, this paper considers minimizing the volume of used permanent magnet as an optimization objective function. In this case, the price difference between AFPM motor and conventional induction motor can be reduced as much as possible. Therefore, the usage of AFPM motors instead of conventional induction motors is economically justified.

By using the PSO algorithm, the dimensions and basic parameters of the slotless axial flux permanent magnet machine with 60° electrical distributed winding are calculated to achieve an almost sinusoidal back EMF. In addition, this algorithm is used to minimize the needed magnet. This optimum design process is done by using MATLAB software. The characteristics of the motor for minimization of magnet weight are given in Table 3.

Now, by using parameters values given in Table 3 and finite element analysis, the designed motor is evaluated.

The machine is constructed by putting identical pole pairs around the axis of the machine. Only one pole pair is considered in the processes of design. Based on this structure, the machine performance is evaluated to reduce the analysis time of the machine. Flux density distributions in the stator and rotor cores for open-circuit conditions are shown in Fig. 3 and Fig. 4, respectively.

Table 3: The basic dimensions and parameters of the designed machine

Parameter	Value	Unit
λ	0.7	-
α	0.6992	-
$B_g(T)$	0.3501	Tesla
$g(mm)$	1	mm
P	5	-
$V_L(V)$	60.44	Volt
$L_{pm}(mm)$	2.8583	mm
A	25598	A/m
D_o	161.53	mm
L_{cs}	10.068	mm
L_{cr}	5.2959	mm
P_{den}	1.3551	W/Cm^2

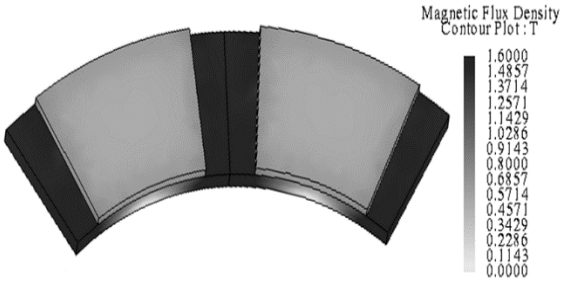

Fig. 3: The flux density distribution of the rotor core

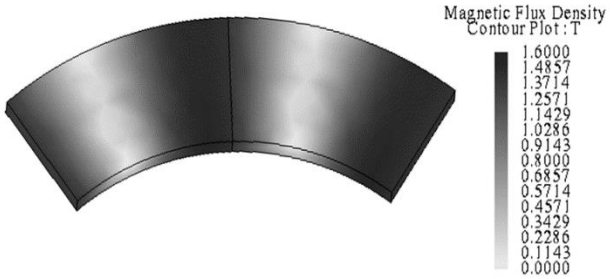

Fig. 4: The flux density distribution of the stator core

The maximum flux densities in the stator and rotor cores are equal to 1.5021 Tesla and 1.4910 Tesla, respectively, which are equal to the values considered at the beginning of the design process. As shown in these figures, no local saturation occurs in the stator and rotor cores.

The air gap flux density of the motor in no-load conditions is shown in Fig. 5. According to the equations presented in the previous section, the magnet thickness and coefficient α have significant impacts on the amplitude and shape of the air gap flux density. In this paper, the magnet thickness is designed to achieve the maximum air gap flux density of 0.5 Tesla and the average air gap flux density of 0.35 Tesla. Furthermore, the FEA results show the maximum air gap flux density of 0.494 Tesla and the average air gap flux density of 0.3409 Tesla, so the equation presented for calculating magnet thickness has high accuracy and the results show that the presented method is effective.

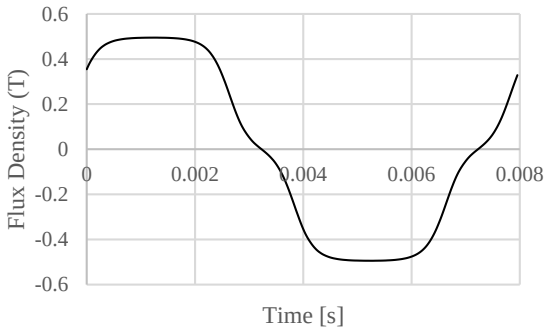

Fig. 5: Air gap flux density

Waveform and the value of the back EMF have a significant influence on almost all performance characteristics of the machine, including power capability, power factor, and torque ripples. The back EMF waveform of the designed machine is shown in Fig. 6. Also, the values of the harmonic component of the back EMF waveforms are presented in Fig. 7. It is clear that the back EMF waveform is almost a pure sinusoidal waveform that results in the reduction of the motor torque fluctuations. Fig. 8 shows the rated torque of the motor. As shown in this figure, the motor torque is almost constant.

The THD reduction of the back EMF waveform reduces the THD of the input current and motor torque fluctuations. For this reason, another optimization objective function is used to reduce the back EMF waveform THD. This is possible by making the air gap flux density sinusoidal and avoiding the saturation of the rotor and stator cores. As shown in Fig. 7, the THD of the back EMF waveform is about 6.4031 percent, reflecting that it is almost sinusoidal and one of the design objectives is accomplished.

According to the results presented in this section, the values obtained from the introduced equations are largely close to FEA results, showing high accuracy of these equations. To better investigate these equations, a comparison has been made in Table 4 between these equation results and FEA results, which confirms the accuracy of the presented scheme.

5. CONCLUSION

This paper presented a new optimization algorithm for the calculation of the basic dimensions of a slotless AFPM machine. The presented equations can be applied to design a machine in such a way that the magnetic flux density throughout the stator and rotor cores remains just below the saturated values. This value is specified by the ferromagnetic material characteristics, which results in using active materials most effectively. To verify the design procedure of the present paper, a sample machine is designed. FEA is carried out for performance evaluations of the machine. The simulation results present the uniform distribution of the flux density inside the cores, which leads to the design of a machine with a lower total iron loss. It is shown that the amplitude of the back EMF is in accordance with the value considered at the beginning of the design algorithm. Also, it is obvious that the back EMF is almost sinusoidal. Some other results have been presented, according to all of which the validity of the proposed design algorithm is confirmed.

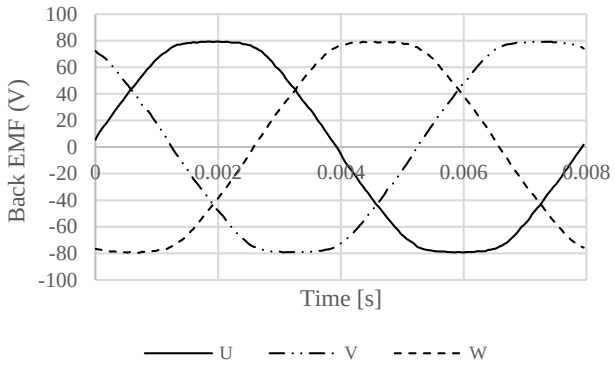

Fig. 6: The induction voltage of the motor

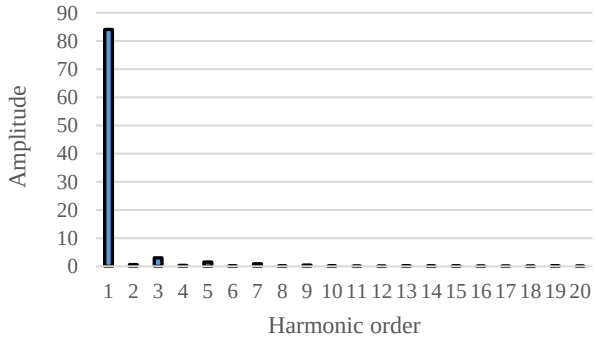

Fig. 7: The harmonics of the induction voltage

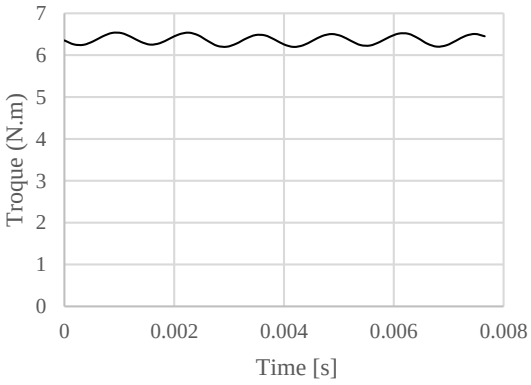

Fig. 8: The rated torque of the motor

Table 4: A comparison of the results obtained from sizing equations and finite element method.

Parameter	FEM	Sizing Equations	Unit
B_g	0.3409	0.35	Tesla
B_{gp}	0.494	0.50	Tesla
B_{cs}	0.9585	0.9549	Tesla
B_{csp}	1.5021	1.5	Tesla
B_{cr}	0.9515	0.9549	Tesla
B_{crp}	1.4910	1.5	Tesla
B_u	0.6044	0.5857	Tesla
I_{ph}	6.016	5.965	A
E_{ph}	119.78	123.18	Volt
K_i	1.3360	1.3485	

DECLARATION OF COMPETING INTEREST

The author declares that he has no known competing financial interests or personal relationships that could have appeared to influence the work reported in this paper. The ethical issues, including plagiarism, informed consent, misconduct, data fabrication and/or falsification, double publication and/or submission, redundancy, have been completely observed by the author.

REFERENCES

[1] A. Mahmoudi, S. Kahourzade, N. Abd Rahim, and W. P. Hew, "Design, analysis, and prototyping of an axial-flux permanent magnet motor based on genetic algorithm and finite-element analysis," *IEEE Transactions on Magnetics*, vol. 49, no. 4, pp. 1479-1492, 2012.

[2] A. Mahmoudi, S. Kahourzade, N. A. Rahim, and H. W. Ping, "Improvement to performance of solid-rotor-ringed line-start axial-flux permanent-magnet motor," *Progress In Electromagnetics Research*, vol. 124, pp. 383-404, 2012.

[3] M. Aydin, and M. Gulec, "Reduction of cogging torque in double-rotor axial-flux permanent-magnet disk motors: A review of cost-effective magnet-skewing techniques with experimental verification," *IEEE Transactions on Industrial Electronics*, vol. 61, no. 9, pp. 5025-5034, 2013.

[4] M. Aydin, and M. Gulec, "A new coreless axial flux interior permanent magnet synchronous motor with sinusoidal rotor segments," *IEEE Transactions on Magnetics*, vol. 52, no. 7, pp. 1-4, 2016.

[5] Daghigh, H. Javadi, and H. Torkaman, "Design optimization of direct-coupled ironless axial flux permanent magnet synchronous wind generator with low cost and high annual energy yield," *IEEE Transactions on Magnetics*, vol. 52, no. 9, pp. 1-11, 2016.

[6] W. Tong, S. Wang, S. Dai, S. Wu, and R. Tang, "A quasi-three-dimensional magnetic equivalent circuit model of a double-sided axial flux permanent magnet machine considering local saturation," *IEEE Transactions on Energy Conversion*, vol. 33, no. 4, pp. 2163-2173, 2018.

[7] G. Yang, M. Lin, N. Li, and L. Hao, "Magnetization state regulation characteristic study of series hybrid permanent magnet axial field flux-switching memory machine," *IEEE Transactions on Applied Superconductivity*, vol. 29, no. 2, pp. 1-6, 2019.

[8] E. Yıldırız, M. Güleç, and M. Aydın, "An innovative dual-rotor axial-gap flux-switching permanent-magnet machine topology with hybrid excitation," *IEEE Transactions on Magnetics*, vol. 54, no. 11, pp. 1-5, 2018.

[9] M. F. Khatab, Z. Zhu, H. Li, and Y. Liu, "Comparative study of novel axial flux magnetically geared and conventional axial flux permanent magnet machines," *CES Transactions on Electrical Machines and Systems*, vol. 2, no. 4, pp. 392-398, 2018.

[10] W. Zhang, X. Liang, and F. Yu, "Fault-tolerant control of hybrid excitation axial field flux-switching permanent magnet machines," *IEEE Transactions on Magnetics*, vol. 54, no. 11, pp. 1-5, 2018.

[11] M. C. Gardner, M. Johnson, and H. A. Toliyat, "Comparison of surface permanent magnet axial and radial flux coaxial magnetic gears," *IEEE Transactions on Energy Conversion*, vol. 33, no. 4, pp. 2250-2259, 2018.

[12] G. Messina, E. T. De Bella, and L. Morici, "HTS axial flux permanent magnets electrical machine prototype: Design and test results," *IEEE Transactions on Applied Superconductivity*, vol. 29, no. 5, pp. 1-5, 2019.

[13] M. Gulec, and M. Aydin, "Magnet asymmetry in reduction of cogging torque for integer slot axial flux permanent magnet motors," *IET Electric Power Applications*, vol. 8, no. 5, pp. 189-198, 2014.

[14] P. Hekmati, R. Yazdanpanah, and M. Mirsalim, "Design and analysis of double-sided slotless axial-flux permanent magnet machines with conventional and new stator core," *IET Electric Power Applications*, vol. 9, no. 3, pp. 193-202, 2015.

[15] Y. Liang, L. Wu, X. Bian, and H. Yu, "The influence of transposition angle on 3-D global domain magnetic field of stator bar in water-cooled turbo-generator," *IEEE Transactions on Magnetics*, vol. 51, no. 11, pp. 1-4, 2015.

[16] S. Kumar, W. Zhao, Z. S. Du, T. A. Lipo, and B.-I. Kwon, "Design of ultrahigh speed axial-flux permanent magnet machine with sinusoidal back EMF for energy storage application," *IEEE Transactions on Magnetics*, vol. 51, no. 11, pp. 1-4, 2015.

[17] S. Huang, J. Luo, F. Leonardi, and T. A. Lipo, "A general approach to sizing and power density equations for comparison of electrical machines," *IEEE Transactions on Industry Applications*, vol. 34, no. 1, pp. 92-97, 1998.

[18] M. Aydin, S. Huang, and T. A. Lipo, "Design and 3D electromagnetic field analysis of non-slotted and slotted TORUS type axial flux surface mounted permanent magnet disc machines," in *2001 IEEE International Electric Machines and Drives Conference*, Cambridge, MA, USA, 2001, pp. 645-651.

[19] D. Wang, C. Peng, D. Xue, D. Zhang, and X. Wang, "Performance assessment and comparative study of a permanent magnet machine with axial flux regulator," *IEEE Transactions on Energy Conversion*, vol. 34, no. 3, pp. 1522-1531, 2019.

BIOGRAPHY

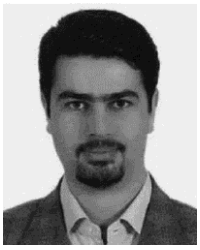

Hamid Radmanesh (Member, IEEE) was born in 1981. He received the B.Sc. degree in electrical engineering from the Malek-Ashtar University of Technology, Tehran, Iran in 2006, the M.Sc. degree in electrical engineering from Shahed University, Tehran, Iran in 2009, and the Ph.D. degree in electrical engineering

from the Amirkabir University of Technology, Tehran, Iran in 2015. He has authored more than 100 published technical papers. His research interests include transient in power systems and renewable energy.